Potential-pulse assisted adsorption of carminic acid dye onto TiO_2 nanoparticles for faster fabrication of higher efficiency sensitized solar cells

J. C. Franco-Gómez[a,⋆], S. Covarrubias-Ortiz[b,⋆], J. Vásquez[b,⋆], R. J. Ortiz-Pérez[a,⋆], E. X. M. García[b], V. H. Romero[a], and A. Estrada-Vargas[b,*]

[a]*Departamento de Ciencias Básicas y Aplicadas, Universidad de Guadalajara, Av. Nuevo Periférico 555, 45425, Tonalá, Jalisco, México.*

[⋆]*These authors contributed equally to this work and share first authorship.*

[b]*Departamento de Estudios del Agua y de la Energía, Universidad de Guadalajara, Av. Nuevo Periférico 555, 45425, Tonalá, Jalisco, México.*

[*]*e-mail: arturo.estrada@cutonala.udg.mx*

Received 20 May 2024; accepted 12 November 2024

Dye adsorption onto the TiO_2 nanoparticles thin film is typically the slowest step in the preparation of dye-sensitized solar cells. Potential assisted adsorption has previously shown to significantly reduce the adsorption time from several hours to minutes. However, it also reduced the cell efficiency in most of the cases and increased it up to 13 % compared to the classical adsorption method, by applying a constant potential for 60 min. In this work, pulsed potential assisted adsorption of carminic acid dye onto TiO_2 nanoparticles significantly reduced the adsorption time and increased the cell efficiency up to 33 % compared to classical adsorption, applying a pulse time of 10 ms and amplitude of 0.5/-0.4 V for 30 min. On the other hand, a single-frequency electrochemical impedance measurement method for monitoring the dye adsorption onto the nanoparticles was tested and provided similar results to the capacitance measurement method. This single-frequency value was determined with the help of relative contribution impedance plots.

Keywords: DSSC efficiency; potential-pulse assisted adsorption; EIS contribution plot.

DOI: https://doi.org/10.31349/RevMexFis.71.021002

1. Introduction

Dye-sensitized solar cells (DSSCs) represent a low-cost and naturally available alternative for generating photovoltaic energy [1]. The TiO_2 nanoparticles thin film of these DSSCs offers a huge area/volume ratio, providing acceptable cell efficiencies.

An important step in DSSCs preparation is the adsorption of the dye onto the TiO_2 film. Typically, the fluorine-doped tin oxide (FTO) photoelectrode coated with the TiO_2 thin film, is dipped into a solution containing the dye and left for several hours until the dye fully covers the TiO_2 surface [2]. The acceleration of this adsorption step is important not only because it allows to shorten DSSCs research time, but also accelerates the mass production of these modified electrodes.

Different efforts in order to accelerate the dye adsorption were summarized by Venkatesan *et al*., where potential-assisted adsorption stands out by its simple and low-cost implementation [3]. Potential assistance decreased the adsorption time from severals hours to minutes, whereas the process also affected the DSSC efficiency. Venkatesan *et al*. applied a selection of constant current/potential and sweeping potential values. The efficiency decreased slightly when comparing with the classical adsorption for most of the cases. However, by applying a constant potential of 3 V for 60 min, the cell efficiency increased 0.3 %. Sivanadaman *et al*. used constant potential assisted adsorption and enhanced the efficiency by 13 % compared to the conventional dye staining method [4].

On the other hand, Jambrec *et al*. tested pulse-potential assisted adsorption in systems such as DNA or thiols onto gold and proven to significantly reduce the adsorption time more efficiently than open-circuit or constant potential experiments [5,6]. The enhanced adsorption has been attributed to a so-called ion-stirring effect on the adsorbing molecules close to the electrode surface.

In this work, we fabricated FTO-TiO_2 electrodes conventionally and performed carminic acid (CA) dye adsorption onto the TiO_2 nanoparticles layer by three different potential methods. First method consisted of adsorption at open-circuit potential (OCP, ca. -0.02 V). Second method consisted of applying constant potentials more positive than OCP, since they should enhance the dye migration towards the TiO_2 surface. Third method consisted of applying pulsed potential of selected pulse times and potential amplitudes, with potential values more positive and a more negative than OCP in order to generate the ion-stirring effect. We selected carminic acid because it is a natural pigment of low production cost and minimal toxicity [7-9]. Efficiencies of solar cells sensitized with this dye range from 0.19 to 1.3 %. We also compared CA adsorption monitoring results by using capacitance and single-frequency impedance measurements.

2. Experimental

FTO photoelectrodes ($10 \times 10 \times 6$ mm, Sigma-Aldrich) were partially covered with 0.5 mm thickness masking tape in order to leave uncovered 0.5 cm width squares. Uncovered

areas were covered first with transparent (10 nm diameter, Sigma-Aldrich) and then with opaque (100 nm diameter, Sigma-Aldrich) TiO_2 nanoparticles paste, following the so-called Dr. Blade method and annealing at 450°C for 2 h [10]. The electrodes were finally cut in smaller rectangular pieces to obtain 1×2 cm FTO electrodes with a 0.5×0.5 cm TiO_2 covered area close to the glass extreme. Electrochemical measurements were made by immersing FTO-TiO_2 modified electrodes as working electrode into a 10 mM carminic acid (Sigma-Aldrich) solution. An Ag/AgCl wire and a Pt mesh were respectively used as pseudoreference and counter electrodes. The control of the electrochemical cell potential and the electrochemical impedance spectroscopy (EIS) measurements were performed with a PalmSens 4 potentiostat. UV-Vis and AFM measurements were performed on the FTO-TiO_2 modified electrodes by using respectively a Jasco V-770 spectrophotometer and a Nanosurf NaioAFM microscope. Solar cells were fabricated by clipping a carminic acid-sensitized electrode and a graphite-impregnated FTO with a 180 ± 30 μm spacer. A 10 mM I_2 / 110 mM KI in 50 % V/V acetic acid solution and was used as electrolyte. Current-voltage measurements of solar cells were performed by exposing them to a 100 mW cm^{-2} light source (ULTRA-VITALUX) and using a variable resistor and two multimeters connected in series and parallel to measure cell current and potential respectively.

3. Results and discussion

Atomic Force Microscopy (AFM) measurements were performed onto transparent and opaque TiO_2 layers without dye. Figures 1a) and 1b) show the AFM height maps. Well defined zones that correspond approximately to the desired particle sizes are shown. Size count for the particles was performed by using the ImageJ® software. Figures 1c) and 1d) show the particle size histograms corresponding to particle count of Figs. 1a) and 1b) respectively. For transparent TiO_2 paste, about 30% of the counts corresponded to particles of diameter between 10 and 20 nm, and the rest distributed over a size range between 0 and 70 nm. For opaque TiO_2 paste, particle size distributed more uniformly over a range of sizes between 10 and 400 nm.

The carminic acid adsorption onto TiO_2 nanoparticles was firstly monitored by performing capacitance measurements. These have been used previously to calculate the percentage of a solid electrode surface that has been covered by adsorbing substances [11,12]. Electrochemical Impedance Spectra (EIS) were recorded every 5 minutes during dye adsorption onto the FTO-TiO_2 modified electrodes. Figure 2a) shows a Nyquist diagram of an EIS spectra of the modified electrode in 5.0 mM carminic acid solution. The spectra were fit by using the Electrical Equivalent Circuit (EEC) shown in Fig. 2b) firstly with the help of the PsTrace® software and then in bulk by using Octave® home-made scripts. This EEC

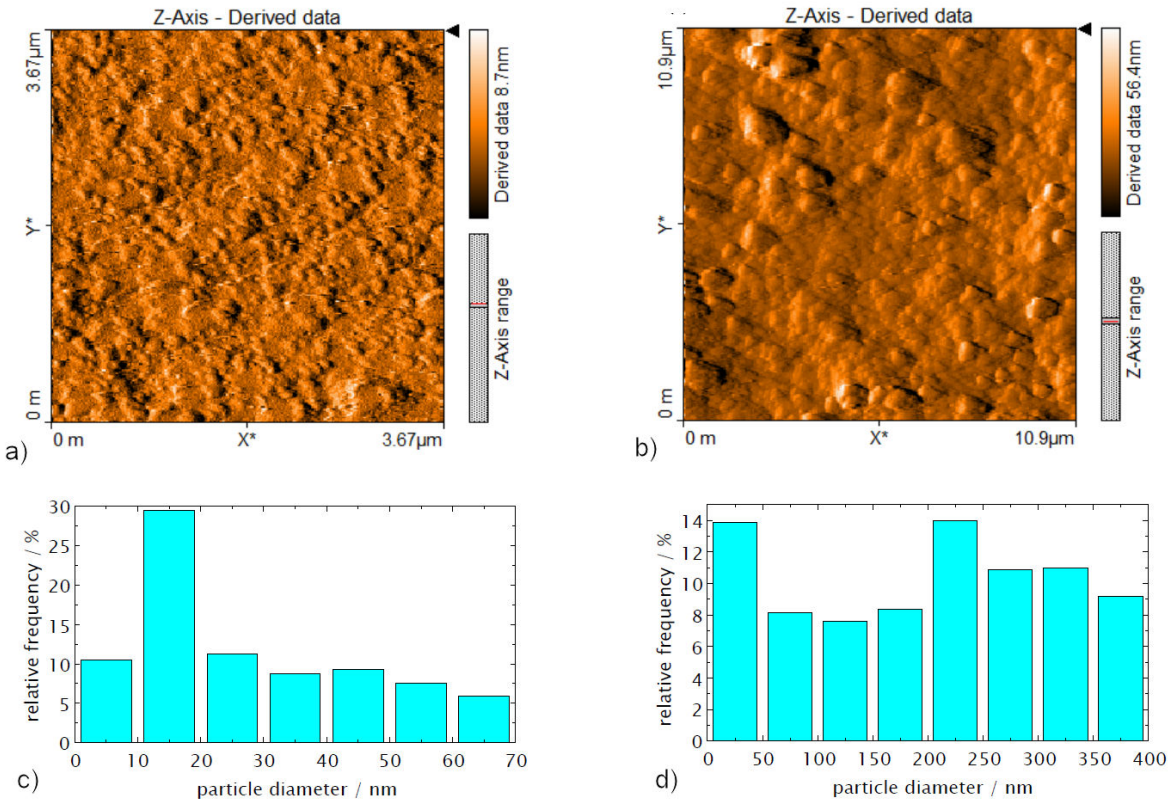

FIGURE 1. AFM maps of a) transparent and b) opaque TiO_2 nanoparticle layers fabricated with Dr. Blade method, and particle size count for same c) transparent and d) opaque layers respectively.

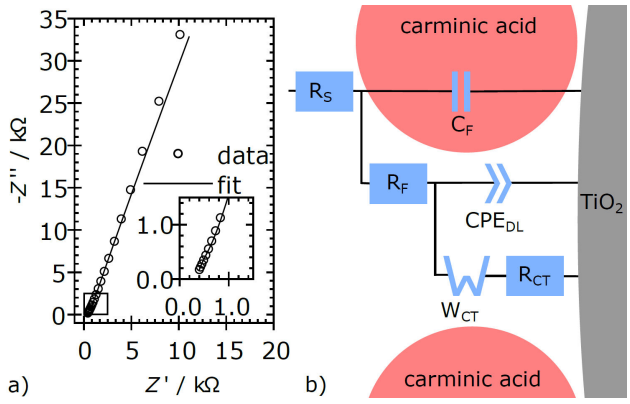

FIGURE 2. (a) Nyquist diagram of EIS spectrum of FTO-TiO_2 modified electrodes immersed in carminic acid and b) electrical equivalent circuit used to fit EIS spectra.

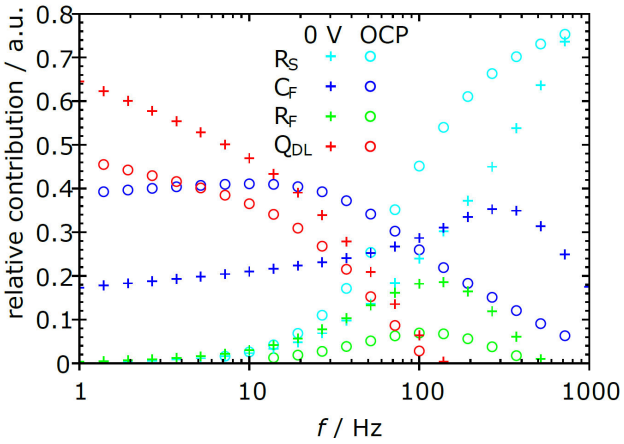

FIGURE 3. Relative contribution plot of selected EEC elements.

has been previously used to represent species adsorption onto solid electrodes [13]. Briefly, R_S is the solution resistance, C_F is the adsorbed dye film capacitance, R_F is the resistance within the film and CPE_{DL} is the Constant Phase Element associated to the double-layer capacitance. W_{CT} and R_{CT} are respectively the diffusion impedance and the charge-transfer resistance associated with faradaic processes which discussion is beyond the scope of this work.

The TiO_2 surface coverage, θ, was associated with the film capacitance by using the formula [12,14]:

$$\theta = \frac{C_F - C_{F0}}{C_{F1} - C_{F0}}, \tag{1}$$

where C_F is the electrode film capacitance value at any time, C_{F0} is the bare TiO_2 nanoparticles capacitance value and C_{F1} is the capacitance value of the TiO_2 fully covered with dye.

A Langmuir model was used to fit the adsorption of carminic acid (CA). Briefly, the adsorption followed the reaction:

$$\mathrm{CA_{(ac)} + S} \underset{k_{\mathrm{des}}}{\overset{k_{\mathrm{ads}}}{\rightleftharpoons}} \mathrm{CA_{(ads)}}, \tag{2}$$

The model follows the adsorption-desorption kinetics:

$$v_{ads} = k_{\mathrm{ads}}[\mathrm{CA_{aq}}][S] = k_{\mathrm{ads}}[\mathrm{CA_{aq}}][S_{\max}](1-\theta), \tag{3}$$

$$v_{des} = k_{\mathrm{des}}[\mathrm{CA_{ads}}] = k_{\mathrm{des}}[S_{\max}](\theta), \tag{4}$$

where k_{ads} and k_{des} are respectively the carminic acid adsorption and desorption kinetic constants and $[S]$ is the concentration of empty adsorption sites onto the TiO_2 surface. The site occupation rate, $v_{\mathrm{ads}} - v_{\mathrm{des}}$, gives a linear differential equation which solution is (after assuming that $[CA_{aq}]$ value is high enough to ensure that $k_{\mathrm{ads}}\,[\mathrm{CA_{aq}}] \gg k_{\mathrm{des}}$):

$$\theta = 1 - e^{-k_{\mathrm{ads}}[\mathrm{CA}_{aq}]t}. \tag{5}$$

Substitution of Eq. (5) onto Eq. (1) results in:

$$C_F = (1 - e^{-k_{ads}[CA_{aq}]t})(C_{F1} - C_{F0}) + C_{F0}, \tag{6}$$

Eq. (6) was used to fit the C_F vs. t data from EIS measurements to obtain parameters k_{ads} and C_{F1}. Therefore, C_{F1} was used to calculate θ using Eq. (1).

Tracking the dye adsorption through time may present experimental constraints for EIS measurements which are not instantly performed, as in Fourier Transform EIS (FTIR-EIS). Also, fitting several impedance spectra recorded during adsorption may consume extra computing time. An alternative to perform multiple impedance spectra consists of performing single-frequency impedance measurements. In order to determine the frequency at which the impedance modulus, $|Z|$, could reflect the CF value, the relative contribution of each EEC element to $|Z|$ was calculated for all EIS frequencies

Figure 3 shows the relative contribution vs. frequency plot of selected EEC elements used to fit the impedance spectra. It can be seen that CF shows a relatively high contribution ca. 72 Hz. At lower and higher frequencies, the $|Z|$ values are respectively dominated by Q_{DL} and R_S. These so-called influence or contribution plots have been previously used to determine work frequencies in order to perform fast impedance measurements with spatial resolution [15,16].

Therefore, Eq. (1) was modified with $|Z|$ values measured at 72 Hz instead of C_F, leading to the formula:

$$\theta = \frac{|Z| - |Z|_0}{|Z|_1 - |Z|_0}. \tag{7}$$

Substituting Eq. (7) on (5) gives a formula to fit $|Z|$ vs. t data to obtain parameters $|Z|_1$ and k_{ads}:

$$|Z| = (1 - e^{-k_{\mathrm{ads}}[CA_{aq}]t})(|Z|_1 - |Z|_0) + |Z|_0. \tag{8}$$

Figure 4 shows a plot of θ vs. t during carminic acid adsorption onto TiO_2. Markers and solid lines represent θ calculated respectively with Eqs. (1) and (7). Typical adsorption at OCP monitored by using Eq. (1) reached a first steady value ca. 50 min and a second steady value ca. 5 h (not shown). Data from EEC fitting (Eq. (1)) shows that pulse and constant potential application reduce the adsorption time to ca. 12 min. However, data from $|Z|$ at 72 Hz [Eq. (7)], shows that adsorp-

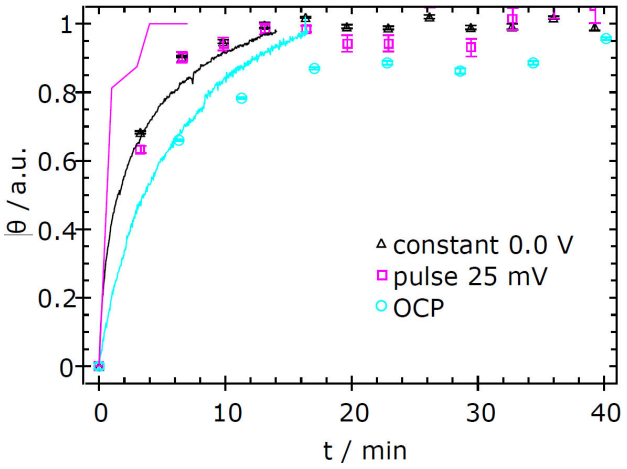

FIGURE 4. Surface coverage of TiO_2 nanoparticles with carminic acid as a function of time for selected potential conditions.

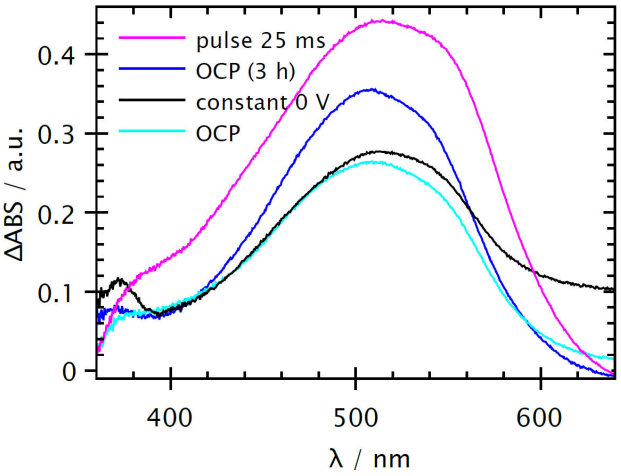

FIGURE 5. Absorbance difference values for carminic acid adsorbed onto TiO_2 nanoparticles at different potential conditions.

TABLE I. Carminic acid adsorption rate constants calculated with Eqs. (6) and (8) for different CA adsorption methods.

equation	OCP	constant	pulse
k_{ads} Eq. (6) / mM^{-1} min^{-1}	0.020	0.035	0.033
k_{ads} Eq. (8) / mM^{-1} min^{-1}	0.0186	0.041	0.18

tion for pulsed potential method reduces the adsorption time to ca. 4 min. This difference between monitoring adsorption with Eqs. (1) and (7) can be due to the limitation of the potentiostat to apply pulsed and alternating voltage simultaneously, and the EIS or $|Z|$ measurements had to be applied interrupting the pulsed potential application.

Table I shows the k_{ads} values from fitting C_F and $|Z|$ vs. t respectively with Eqs. (6) and (8). The k_{ads} value from Eq. (6) for pulsed and constant potential methods are similar, suggesting they accelerate adsorption to similar rates. However, k_{ads} from Eq. (8) shows a value for pulse potential method four times the one obtained for constant potential method.

Ultraviolet-visible spectroscopy (UV-vis) was performed on modified FTO-TiO_2 electrodes to evaluate the increase of light absorbance due to the presence of carminic acid. An absorbance peak at a wavelength on the 497∼510 nm range has been reported previously for this dye adsorbed onto TiO_2 [17,18].

Figure 5 shows the absorbance difference values for FTO-TiO_2 modified electrodes after adsorbing carminic acid by the compared potential methods for 15 min adsorption time. The difference values were obtained by subtracting the absorbance of a FTO-TiO_2 modified electrode prior to carminic acid adsorption. The absorbance difference with a typical 3 h adsorption time at OCP is also shown. The absorbance difference values ca. 510 nm for OCP and constant potential methods for 15 min were smaller than that for typical adsorption. However, pulse potential method showed a greater absorbance difference value. We assumed that ion-stirring effect due to the application of potential pulses could allow more carminic acid molecules to arrange close to the TiO_2 surface, compared to the other methods. We considered the ion-stirring effect existed since a considerable fraction of the potential drop between spherical nanoparticles and a counter-electrode occurs close to the particles surface [19,20]. However, a more detailed study by using other analytic techniques should be performed as future work.

TABLE II. Parameters of DSSCs fabricated with pulsed-potential adsorption steps of different pulse times.

pulse time / ms	FF	V_{oc}/V	I_{sc}/mA	η/%
10	0.21	0.39	0.34	0.028
100	0.23	0.35	0.16	0.013

In order to compare DSSC efficiency, selected pulse durations and amplitudes were tested. Table II shows the efficiency of DSSCs prepared with carminic acid adsorption pulse amplitude of 0.3/-0.2 V and duration of 10 and 100 ms for 30 min. The efficiency was greater for the DSSC prepared with 10 ms pulse. Jambrec *et al.* obtained also a similar optimal pulse time value for thiols adsorption onto gold by comparing pulse durations in a range from 1 to 10 000 ms [6]. Therefore, a pulse time of 10 ms was used for experiments at selected pulse potential amplitudes.

Figure 6 shows plots the current-potential plots for DSSCs fabricated with 30 min dye adsorption step at selected potential conditions and compared to OCP adsorption for 24 h. Dots represent experimental data and lines the fitting to Eq. (9):

$$i = i_{sc} - i_0 \left(e^{\frac{V+iR_s}{V_t}} - 1 \right) - \frac{V + iR_s}{R_{sh}}, \qquad (9)$$

where R_s and R_{sh} are the fit values of the series and shunt resistance of the DSSC and i_0 the dark current. Table III shows a comparison of DSSC efficiencies of selected potential conditions.

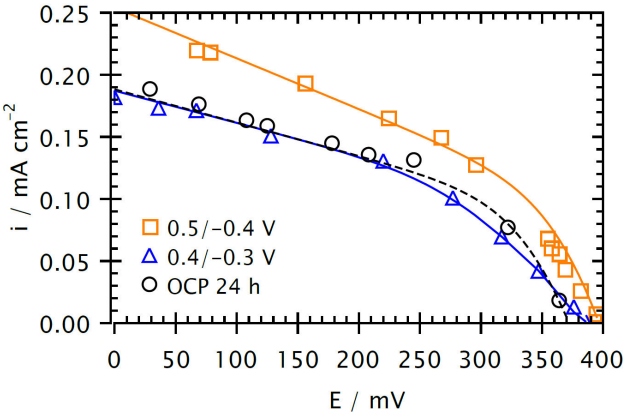

FIGURE 6. Current-potential plot for DSSCs fabricated with selected CA adsorption potentials.

TABLE III. Parameters of DSSCs fabricated with 30 min adsorption step at different potential conditions. Maximum η deviation was 0.003 %.

potential method	FF	V_{oc} / V	i_{sc} / mA cm^{-2}	η / %
OCP 24 h	0.32	0.45	0.25	0.030
constant 0.3 V	0.27	0.32	0.14	0.012
constant 3.0 V	0.24	0.29	0.17	0.012
pulse 0.3/-0.2 V	0.21	0.39	0.34	0.028
pulse 0.4/-0.3 V	0.34	0.39	0.22	0.029
pulse 0.5/-0.4 V	0.35	0.40	0.28	0.039

The obtained efficiencies were one order smaller than those obtained for carminic acid DSSCs in previous works [8,9]. We attributed this result to the different counter-electrode utilized in this work, the large separation between the modified and the counter electrodes and the relatively large TiO_2 film thickness, which resulted in high R_s values ranging from 180 to 750 Ω cm^2 and therefore small DSSC fill factors and efficiencies [21]. R_{sh} values ranged from 1 440 to 3 280 Ω cm^2 and were considered high enough to not affect negatively the DSSC efficiencies, although a small tilt can be noticed in the $i-V$ curves of Fig. 6 at potential values close to 0.

The DSSC efficiencies using the constant potential adsorption method were smaller than half the value obtained with 24 h classical adsorption, whereas Venkatesan *et al.* achieved an efficiency 0.3 % higher than the obtained with the traditional method, by applying 3 V for 60 min [3]. Efficiencies obtained with the pulse-potential adsorption method showed a trend to increase with the pulse amplitude. Although they are smaller than the obtained in previous works, it should be noticed that the efficiency obtained with the 0.5/-0.4 V pulse was 33 % higher compared to the traditional adsorption techinque, whereas the highest increment previously reported with potential-assisted adsorption was 13 %, achieved by Sivanadanam *et al.* by applying a constant potential [4].

This work presents results only for enhanced adsorption of carminic acid onto TiO_2 for a small selection of potential pulse-conditions. Dye anchoring functional groups and orientation onto the TiO_2 nanoparticles layer are expected to have effects on the values of recombination resistances and hence the cell efficiency, as observed before for other dyes. Adsorption mechanisms were proposed for MK-2, MK-44, N719 and triphenylamine-based dyes, for example [22-24]. Although carminic acid has several functional groups with potential to bind to the TiO_2 layer, we did not find any anchoring or orientation study for this dye. This study is neccesary and should be performed as future work. Meanwhile, we assumed the so-called ion-stirring effect could affect the anchoring functional group and hence the orientation and compactness of carminic acid molecules onto the TiO_2 layer. In any case, the obtained results in this work open the posibility to enhance the efficiencies of already existing DSSCs, and we encourage the scientific community to test potential-pulse assisted adsorption of other dyes.

4. Conclusions

Adsorption of carminic acid dye onto TiO_2 nanoparticles was assisted with the application of constant and pulsed potential. Adsorption was monitored by electrochemical impedance spectroscopy and single-frequency impedance measurements. The obtained kinetic adsorption constants were greater for constant or pulsed potential methods than for classic adsorption method for both monitoring techniques.

UV-vis spectroscopy measurements showed a greater adsorpted amount of CA onto TiO_2 by performing the pulsed potential method, compared to constant and open-circuit potential methods.

Efficiencies for CA DSSCs prepared with the pulse-potential adsorption method ranged from 14 % smaller to 33 % greater than those prepared with the traditional adsorption method, for the studied pulse durations and amplitudes.

Acknowledgements

The authors are grateful for financial support from Secretaría de Educación Pública, (SEP, México), through grant UDG-PTC-1408.

1. A. Hagfeldt and M. Grätzel, Molecular Photovoltaics, Accounts of Chemical Research **33** (2000) 269, https://doi.org/10.1021/ar980112j.
2. D. Rangel *et al.*, Optimized dye-sensitized solar cells: A comparative study with different dyes, mordants and construction parameters, Results in Physics **12** (2019) 2026, https://doi.org/10.1016/j.rinp.2019.01.096.
3. S. Venkatesan *et al.*, Enhanced adsorption on TiO2 photoelectrodes of dye-sensitized solar cells by electrochemical methods dye, *Journal of Alloys and Compounds* **903** (2022) 163959, https://doi.org/10.1016/j.jallcom.2022.163959.
4. J. Sivanadanam, I. S. Aidhen, and K. Ramanujam, New cyclic and acyclic imidazole-based sensitizers for achieving highly efficient photoanodes for dye-sensitized solar cells by a potentialassisted method, *New Journal of Chemistry* **44** (2020) 10207, https://doi.org/10.1039/d0nj00137f.
5. D. Jambrec *et al.*, Potential-Assisted DNA Immobilization as a Prerequisite for Fast and Controlled Formation of DNA Monolayers, *Angewandte Chemie* **127** (2015) 15278, https://doi.org/10.1002/ange.201506672.
6. D. Jambrec *et al.*, Potential-Pulse-Assisted Formation of Thiol Monolayers within Minutes for Fast and Controlled Electrode Surface Modification, *Chem. Electro. Chem.* **3** (2016) 1484, https://doi.org/10.1002/celc.201600308.
7. S. H. Aung *et al.*, Kinetic study of carminic acid and santalin natural dyes in dye-sensitized solar cells, *Journal of Photochemistry and Photobiology A: Chemistry* **325** (2016) 1, https://doi.org/10.1016/j.jphotochem.2016.03.022.
8. Y. Kocak and A. Yildiz, Carminic acid extracted from cochineal insect as photosensitizer for dye-sensitized solar cells, International *Journal of Energy Research* **45** (2021) 16901, https://doi.org/10.1002/er.6883.
9. A. Orona-Navar *et al.*, Photoconversion efficiency of Titania solar cells co-sensitized with natural pigments from cochineal, papaya peel and microalga Scenedesmus obliquus, *Journal of Photochemistry and Photobiology A: Chemistry* **388** (2020) 112216, https://doi.org/10.1016/j.jphotochem.2019.112216.
10. A. I. Kontos, et al., Nanostructured TiO2 films for DSSCS prepared by combining doctor-blade and sol-gel techniques, *Journal of Materials Processing Technology* **196** (2008) 243, https://doi.org/10.1016/j.jmatprotec.2007.05.051.
11. R. Subramanian and V. Lakshminarayanan, Study of kinetics of adsorption of alkanethiols on gold using electrochemical impedance spectroscopy, *Electrochimica Acta* **45** (2000) 4501, https://doi.org/10.1016/S0013-4686(00)00512-0.
12. D. G. Georganopoulou *et al.*, Effect of nonionic surfactants on interfacial electron transfer at the liquid/liquid interface, *Langmuir* **17** (2001) 8348, https://doi.org/10.1021/la0108499.
13. M. A. Macdonald and H. A. Andreas, Method for equivalent circuit determination for electrochemical impedance spectroscopy data of protein adsorption on solid surfaces, *Electrochimica Acta* **129** (2014) 290, https://doi.org/10.1016/j.electacta.2014.02.046.
14. B. B. Damaskin, O. A. Petrii, and V. V. Batrakov, Adsorption of organic compounds on electrodes (Plenum Press, 1971).
15. A. Estrada-Vargas *et al.*, In Situ Characterization of Ultrathin Films by Scanning Electrochemical Impedance Microscopy, *Analytical Chemistry* **88** (2016) 3354, https://doi.org/10.1021/acs.analchem.6b00011.
16. A. Estrada-Vargas *et al.*, Differentiation between Single- and Double-Stranded DNA through Local Capacitance Measurements, *Chem. Electro. Chem.* **3** (2016) 855, https://doi.org/10.1002/celc.201600075.
17. S. Gaweda, G. Stochel, and K. Szaciłowski, Photosensitization and photocurrent switching in carminic acid/titanium dioxide hybrid material, *Journal of Physical Chemistry C* **112** (2008) 19131, https://doi.org/10.1021/jp804700d.
18. S. Munir *et al.*, Adsorption of porphyrin and carminic acid on TiO2 nanoparticles: A photo-active nano-hybrid material for hybrid bulk heterojunction solar cells, *Journal of Photochemistry and Photobiology B: Biology* **153** (2015) 397, https://doi.org/10.1016/j.jphotobiol.2015.10.029.
19. F. F. Dall'Agnol and V. P. Mammana, Solution for the electric potential distribution produced by sphere-plane electrodes using the method of images, *Revista Brasileira de Ensino de Fisica* **31** (2009) 3503.1, https://doi.org/10.1590/S1806-11172009005000004.
20. P. C. Chaumet and J. P. Dufour, Electric potential and field between two different spheres, *Journal of Electrostatics* **43** (1998) 145, https://doi.org/10.1016/S0304-3886(97)00170-8.
21. N. Kutlu, Investigation of electrical values of low-efficiency dye-sensitized solar cells (DSSCs), *Energy* **199** (2020) 117222, https://doi.org/10.1016/j.energy.2020.117222.
22. J. McCree-Grey *et al.*, Dye TiO_2 interfacial structure of dye-sensitised solar cell working electrodes buried under a solution of I-/I3- redox electrolyte, *Nanoscale* **9** (2017) 11793, https://doi.org/10.1039/c7nr03936k.
23. J. Singh *et al.*, XPS, UV-Vis, FTIR, and EXAFS studies to investigate the binding mechanism of N719 dye onto oxalic acid treated TiO2 and its implication on photovoltaic properties, *Journal of Physical Chemistry C* **117** (2013) 21096, https://doi.org/10.1021/jp4062994.
24. B. G. Kim, K. Chung, and J. Kim, Molecular design principle of all-organic dyes for dye-sensitized solar cells, *Chemistry-A European Journal* **19** (2013) 5220, https://doi.org/10.1002/chem.201204343.